# Synthesis and Characterization of Silver Hollandite and Its Application in Emission Control

Liyu Li and David L. King*

*Materials Division, Pacific Northwest National Laboratory, Post Office Box 999, Richland, Washington 99354*

*Received March 24, 2005*

Silver hollandite, $Ag_{1.8}Mn_8O_{16}$, has been synthesized by ion exchange of cryptomelane in $AgNO_3$ melt. Compared to the previously described synthesis process, thermal decomposition of $AgMnO_4$ at 970 °C under 5 kbar oxygen for 7 days, this newly developed synthesis process is easily carried out, enabling synthesis of significant quantities for evaluation, testing, and scale-up. Silver hollandite prepared by this new method has much smaller crystal size and thus much higher surface area compared with the previously available material. Application of silver hollandite for emission control has been examined. This material is an excellent low-temperature $SO_2$ absorbent as well as a highly active catalyst for CO and NO oxidation. Silver hollandite maintains its catalytic oxidation activity even while it is simultaneously aging by adsorption of $SO_2$.

## Introduction

Hollandite-type manganese oxide materials are of considerable interest because they can be used as oxidation catalysts,[1,2] ion exchangers,[3,4] solid ionic conductors,[5] radioactive waste immobilization,[6] and battery materials.[7] These materials, also referred to as octahedral molecular sieves, are constructed of double chains of edge-sharing $MnO_6$ octahedra forming square cross-section tunnels with two $MnO_6$ on each side.[8−10] The pore diameter of the tunnel is about 0.46 nm. The tunnels are partially filled with uni- or divalent cations such as $Ba^{2+}$ (defined as hollandite), $K^+$ (cryptomelane), $Na^+$(manjiroite), and $Pb^{2+}$ (coronadite). Generally, these cations are located in the center of the cubic cage formed by four $MnO_6$ octahedra, coordinated with eight oxygen anions at a bond distance of about 0.28 nm (see Figure 1 a). The charge on the tunnel cations is balanced by substitution of lower valence $Mn^{3+}$ (or optionally other cations, such as $Fe^{3+}$ and $Al^{3+}$), for some of the $Mn^{4+}$ in the framework.

Preparation of hollandite-type materials has been explored extensively. Reflux methods,[11−13] solid-state high-temperature−high-pressure methods,[6,14,15] and sol−gel methods[1,16,17] are most frequently used to produce hollandite materials. Other metal cations can be introduced into the tunnel by post ion exchange[2,4] or into the framework by substitution during synthesis.[11,12]

Chang and Jansen[18,19] have provided the first and only reported synthesis of Ag-hollandite. In their process, Ag-hollandite ($Ag_{1.8}Mn_8O_{16}$) is prepared from a mixture of $AgMnO_4$ and $Ag_2O$ in the molar ratio 1:1 at 970 °C under 5 kbar oxygen over 7 days. They obtained needlelike crystals with dimensions $0.1 \times 0.4 \times 1.0$ mm$^3$. The structure of Ag-hollandite is different from that of the traditional hollandite in that the silver cations do not occupy the centers of the cubic cages formed by $MnO_6$ octahedra, but rather the common faces of the cubes, coordinated with four oxygen anions at about 0.24 nm (see Figure 1 b). This modification of the structure may contribute to some unique ion conductive and oxidative catalytic properties. More than 20 years have passed and no further characterization work or application has been reported for this material. This is probably due to two factors: (1) the high-temperature, high-pressure syn-

* To whom correspondence should be addressed. E-mail: david.king@pnl.gov. Tel.: 509-375-3908. Fax: 509-375-2186.

(1) Liu, J.; Son, Y. C.; Cai, J.; Shen, X. F.; Suib, S. L.; Aindow, M. *Chem. Mater.* **2004**, *16*, 276−285.
(2) Xia, G. G.; Yin, Y. G.; Willis, W. S.; Wang, J. Y.; Suib, S. L. *J. Catal.* **1999**, *185*, 91−105.
(3) Feng, Q.; Kanoh, H.; Miyai, Y.; Ooi, K. *Chem. Mater.* **1995**, *7*, 148−153.
(4) Dyer, A.; Pillinger, M.; Newton, J.; Harjula, R.; Möller, T.; Amin, S. *Chem. Mater.* **2000**, *12*, 3798−3804.
(5) Beyeler, H. U. *Phys. Rev. Lett.* **1976**, *37*, 1557−1560.
(6) Ringwood, A. E.; Kesson, S. E.; Ware, N. G.; Hibberson, W.; Major, A. *Nature* **1979**, *278*, 219−223.
(7) Dai, J. X.; Li, S. F. Y.; Siow, K. S.; Gao, Z. Q. *Electrochim. Acta* **2000**, *45* (14), 2211−2217.
(8) Vicat, J.; Fanchon, E.; Strobel, P.; Qui, D. T. *Acta Crystallogr.* **1986**, *B42*, 162−167.
(9) Post, J. E.; Von Dreele, R. B.; Buseck, P. R. *Acta Crystallogr.* **1982**, *B38*, 1056−1065.
(10) Byström, A.; Byström, A. M. *Acta Crystallogr.* **1950**, *3*, 146−154.
(11) DeGuzman, R. N.; Shen, Y. F.; Neth, E. J.; Suib, S. L.; O'Young, C. L.; Levine, S.; Newsam, J. M. *Chem. Mater.* **1994**, *6*, 815−821.
(12) Chen, X.; Shen, Y. F.; Suib, S. L.; O'Young, C. L. *Chem. Mater.* **2002**, *14*, 940−948.
(13) Feng, Q.; Horiuchi, T.; Mitsusio, T.; Yanagisawa, K.; Yamasaki, N. *J. Mater. Sci. Lett.* **1999**, *18*, 1375−1378.
(14) Kesson, S. E. *Radioact. Waste Manage. Nucl. Fuel Cycle* **1983**, *4* (1), 53−72.
(15) Hartman, J. S.; Vance, E. R.; Power, W. P.; Hanna, J. V. *J. Mater. Res.* **1998**, *13* (1), 22−27.
(16) Hong, X. L.; Zhang, G. Y.; Zhu, Y. Y.; Yang, H. Q. *Mater. Res. Bull.* **2003**, *38*, 1695−1703.
(17) Sugantha, M.; Ramakrishnan, P. A.; Hermann, A. M.; Warmsingh, C. P.; Ginley, D. S. *Int. J. Hydrogen Energy* **2003**, *28*, 597−600.
(18) Chang, F. M.; Jansen, M. *Rev. Chim. Minëral.* **1986**, *23*, 48−54.
(19) Chang, F. M.; Jansen, M. *Angew. Chem., Int. Ed. Engl.* **1984**, *23* (11), 906−907.

10.1021/cm0506508 CCC: $30.25 © 2005 American Chemical Society
Published on Web 07/20/2005

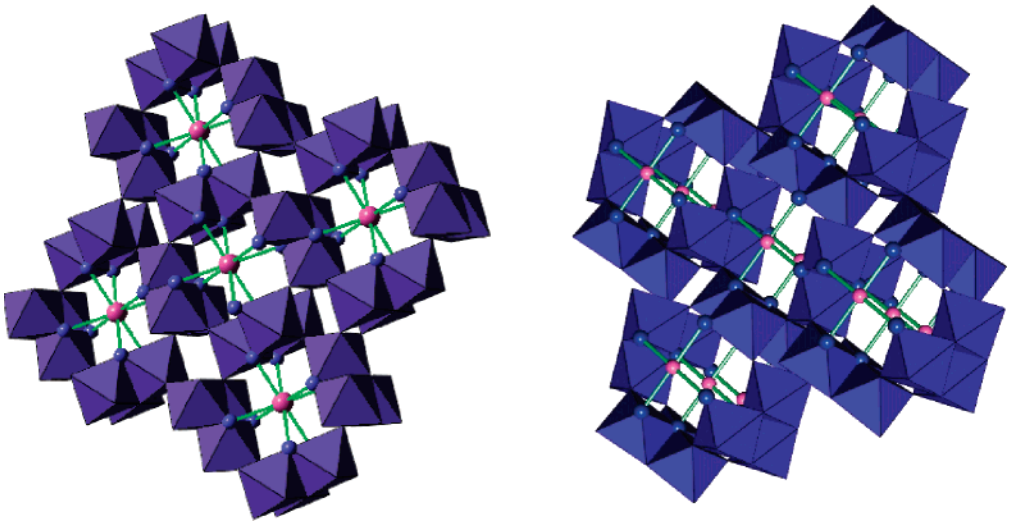

**Figure 1.** Schematic showing $K^+$ position in cryptomelane (left) and $Ag^+$ position in Ag-hollandite (right). $MnO_6$ octahedra are shown in blue. K−O bond length is 0.28 nm and Ag−O bond length is 0.24 nm.

theses process makes it difficult to produce this material in large quantity; (2) the material is not effective for applications such as absorption or catalysis since the large crystal size results in a very low available surface area.

$Ag^+$ cations can be doped into the tunnel structure of cryptomelane by ion exchange. In fact, cryptomelane is very effective for selective adsorption of $Ag^+$ from low pH solutions, even in the presence of large amounts of other cations.[4] After $Ag^+$ ion exchange, the original cryptomelane crystal structure disappears, and a poorly crystallized Ag-hollandite forms.[2]

Here we report a new process that can be used to synthesize highly crystalline, high surface area Ag-hollandite, based on ion exchange of cryptomelane in $AgNO_3$ melt. Some unique applications of this material in emission control, such as low-temperature $SO_2$ absorption and CO and NO oxidation, will also be described.

## Experimental Section

**1. Ag-Hollandite Synthesis and Characterization.** Ag-hollandite was synthesized through post ion exchange treatment of cryptomelane. The cryptomelane was prepared using the method by DeGuzman et al.[11] A typical post ion exchange treatment of cryptomelane was as follows (denoted as method A): 1.0 g of cryptomelane was added to 100 mL of 1 M $AgNO_3$ solution, and the mixture was put into a temperature-controlled shaker and heated to 55 °C under continuous shaking. The total ion exchange duration was 24 h. The liquid was decanted, and the solid was dried in air at 120 °C overnight, resulting in an excess of $AgNO_3$ being present. The dried powder was calcined in air at 500 °C for 2 h. The yield was 1.3 g. An alternate method used was as follows (denoted as method B): 2.0 g of cryptomelane was added to 20 mL of 1 M $AgNO_3$ solution, and then the mixture was put into a temperature-controlled furnace and heated to 150 °C for 3 h and then to 250 °C for 12 h. After ion exchange treatment, extra $AgNO_3$ was washed off using deionized water. The yield of dried powder was 2.54 g.

Powder XRD diffraction measurements were conducted with a Philips PW3050 diffractometer using Cu Kα radiation and JADE, a commercial software package. Sample powders were mounted in a front-loading, shallow-cavity zero-background quartz holder, and the data were collected from 5° to 75° $2\theta$ in step-scan mode using steps of 0.02°. The nitrogen BET surface area was measured with a QUANTACHROME AUTOSORB 6-B gas sorption system with degassed samples. Transmission electron microscopy (TEM) analysis was carried out on a JEOL JEM 2010F microscope. Selected area energy dispersive X-ray spectroscopy (EDS) was performed on regions of interest using a Links EDS system equipped on the microscope. To obtain TEM images, the as-synthesized powder was dispersed in acetone solution and then deposited on a Cu-carbon grid.

The Ag, K, and Mn concentration in cryptomelane and Ag-hollandite were analyzed using an Optima 3000 DV Perkin-Elmer inductively coupled plasma-atomic emission spectrometer (ICP-AES). For ICP elemental analysis, about 20 mg of solid powder was dissolved in 12 mL of 2% $HNO_3$−30% $H_2O_2$ water solution. The mixture was then diluted 1000 times with 2% $HNO_3$ before ICP chemical analysis.

An AMI-200R-HP system (Altamira Instruments, Pittsburgh, PA) was used for temperature-programmed reduction (TPR) measurement. About 50 mg of cryptomelane and Ag-hollandite samples were treated in 60 mL/min 10% $H_2$−90% Ar mixture from room temperature to 600 °C at a heating rate of 10 °C/ min.

The oxidation state of Ag in the product was measured by X-ray photoelectron spectrometry (XPS). A Physical Electronics Quantum 2000 Scanning ESCA Microprobe system was used for the analysis.

**2. $SO_2$ Uptake and CO and NO Oxidation Measurements.** The test setup employed a small fixed bed quartz tube reactor, which was heated by a small clam-shell furnace. Reactant gases were metered using mass flow controllers. For different runs, different feed gases were utilized. The $SO_2$ analytical system comprised a HP6890 gas chromatograph equipped with a Sulfur Chemiluminescent Detector (SCD), which has been described in detail previously.[20] The concentrations of CO and $CO_2$ were measured using an Agilent Quad Series Micro GC. The NO, $NO_2$, and total $NO_x$ were measured using a 600-HCLD Digital $NO_x$ Meter (California Analytical Instruments, Inc.). During the experimental run the analytical system was operated continuously, sampling the effluent every 3 min. The maximum sensitivity of the system to $SO_2$ (with $SO_2$ feed levels 10 ppm) was approximately 50 ppb and approximately 5 ppm for CO, $CO_2$, NO, and $NO_2$. Typical measurements employed a 0.2 g 40−80 mesh particle sample. Each sample was pretreated in flowing air (100 sccm) at 500 °C for 2 h prior to measuring $SO_2$ uptake and oxidation performance.

(20) Li, L. Y.; King, D. L. *Ind. Eng. Chem. Res.* **2004**, *43*, 4452−4456.

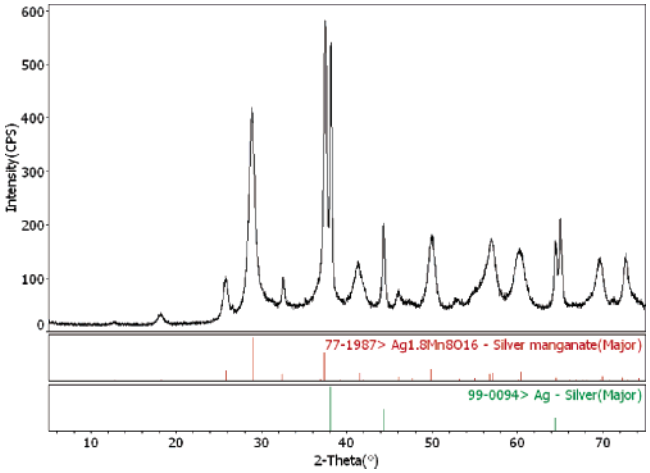


**Figure 2.** XRD pattern of Ag-hollandite from method A (Ag-hollandite A).

## Results and Discussion

**1. Ag-Hollandite Synthesis and Characterization.** Highly crystalline Ag-hollandite (Ag-hollandite A) was obtained using synthesis method A as described in the Experimental Section, i.e., ion exchange with $AgNO_3$ at 55 °C followed by calcination at 500 °C without an intermediate wash of the dried product to remove excess silver nitrate. Figure 2 shows the XRD pattern of the product, and Figure 3 shows its TEM images along with the selected area energy dispersive X-ray spectrum. Table 1 gives the cation composition from ICP-AES measurement.

The XRD pattern matches very well with that of Ag-hollandite, $Ag_{1.8}Mn_8O_{16}$. A certain amount of metallic Ag also exists in the final product, which comes from the decomposition of extra $AgNO_3$ during the high-temperature

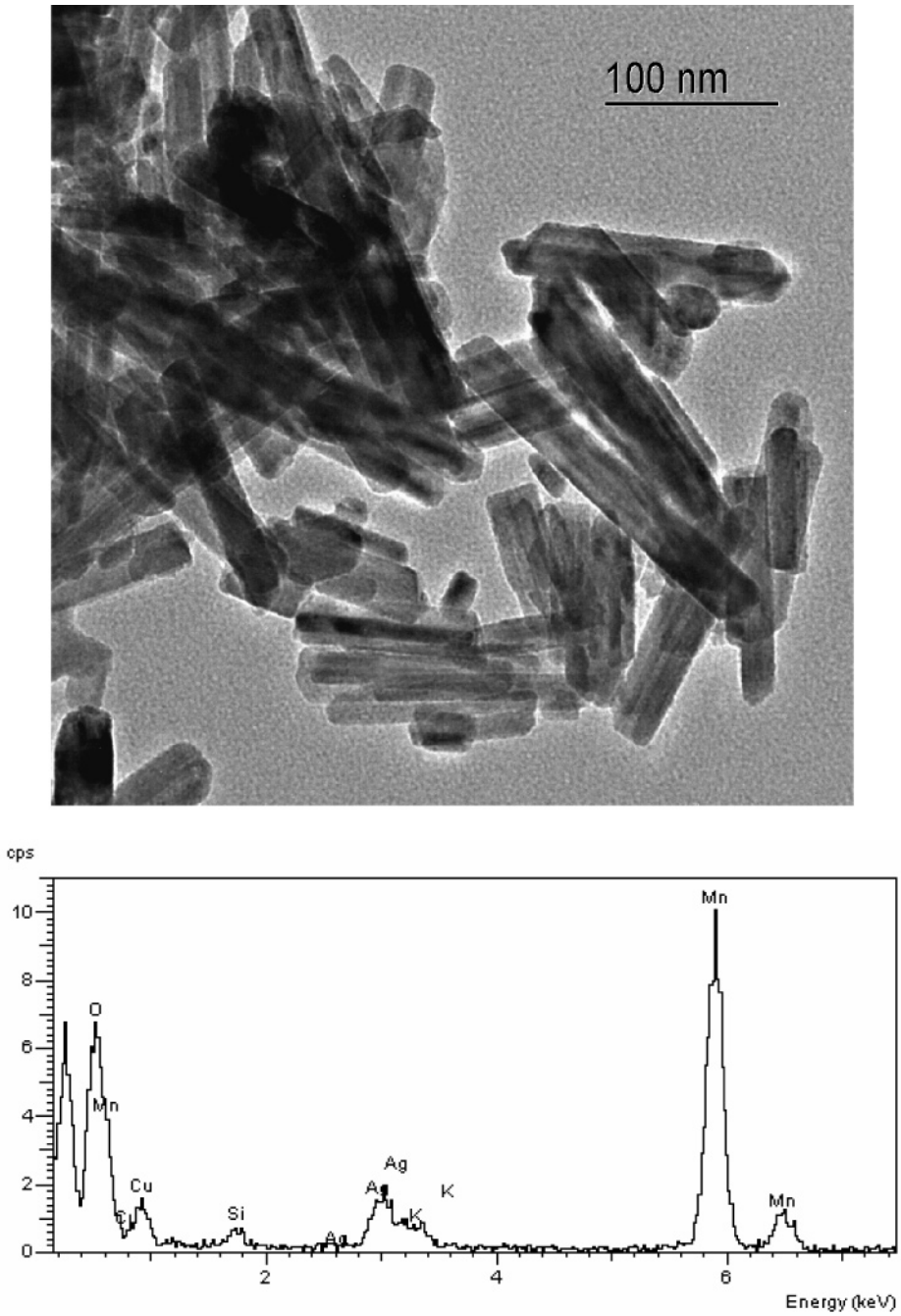


**Figure 3.** TEM image (top) and a typical EDS spectrum (bottom) of Ag-hollandite from method A (Ag-hollandite A).

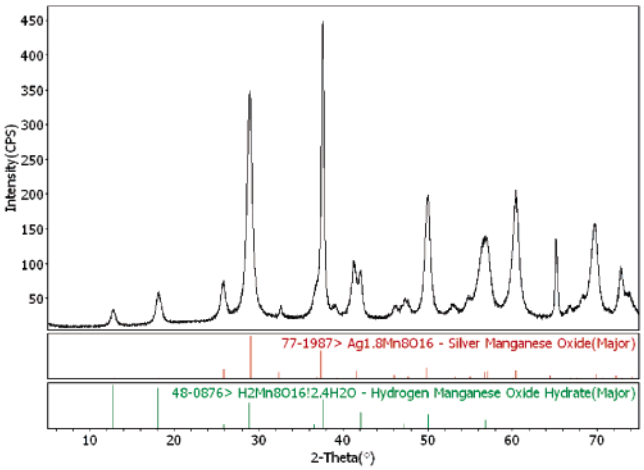


**Figure 4.** XRD pattern of Ag-hollandite washed with 2 M $HNO_3$.

**Table 1. Cation Molar Composition of Cryptomelane and Ag-Hollandite**

| sample | K% | Ag% | Mn% |
|---|---|---|---|
| cryptomelane | 7.25 | 0 | 92.75 |
| Ag-hollandite A | 3.95 | 21.38 | 74.67 |
| water-washed Ag-hollandite A | 3.72 | 19.01 | 77.26 |
| acid-washed Ag-hollandite A | 3.03 | 8.07 | 88.89 |
| Ag-hollandite B | 1.52 | 21.22 | 77.26 |

calcination. These Ag particles are so large that they are visible to the naked eye. The crystal size of Ag-hollandite is much smaller. The crystals are needlelike, ~30 nm width and 100−200 nm long. This morphology is quite similar to that of the cryptomelane starting material, except that the Ag-hollandite crystals are shorter. The EDS spectrum and ICP analysis both show that there is still a small amount of $K^+$ in the crystal structure, which indicates the ion exchange process is not complete. This also indicates that the Ag-hollandite crystal structure can accommodate a small amount of $K^+$. The BET surface area of the as-synthesized material is 35 $m^2/g$, consistent with the small crystallite size.

In an attempt to remove the metallic silver component, the Ag-hollandite A product was treated with 2 M $HNO_3$ solution. The silver phase can be removed, but a fraction of the original product is converted to $H^+$-hollandite (Figure 4). ICP results clearly show that the amount of silver in this sample is much less than that in the original Ag-hollandite A. This indicates that the $Ag^+$ cations inside the tunnel structure of Ag-hollandite can be easily removed and replaced by $H^+$ cations, and the Ag-hollandite structure can easily convert to the H-hollandite structure. Like $K^+$ cations in cryptomelane, $H^+$ cations in H-hollandite are also located in the center of the cubic cage formed by four $MnO_6$ octahedra. Thus, we were unsuccessful in using an acid wash to purify the Ag-hollandite A of excess metallic silver.

In another attempt to remove the extra silver phase from Ag-hollandite A, the silver cation-exchanged cryptomelane was washed with deionized water followed by a final calcination at 500 °C. The XRD pattern of this sample shows a predominance of cryptomelane. This result is quite similar to that obtained from the intermediate product Ag-hollandite from method A, i.e., cryptomelane ion exchanged in 1 M $AgNO_3$ at 55 °C, washed with deionized water to remove excess $AgNO_3$, and dried at 120 °C in air without a subsequent 500 °C calcination (Figure 5). When the silver

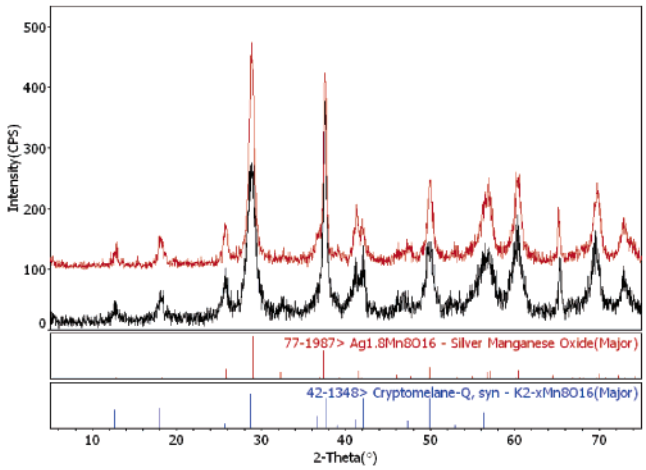


**Figure 5.** Top: XRD pattern of cryptomelane ion-exchanged in 1 M $AgNO_3$ at 55 °C, washed to remove excess $AgNO_3$, and calcined at 500 °C. Bottom: XRD pattern of cryptomelane ion-exchanged in 1 M $AgNO_3$ at 55 °C, washed to remove excess $AgNO_3$, and dried at 110 °C, with no final calcination.

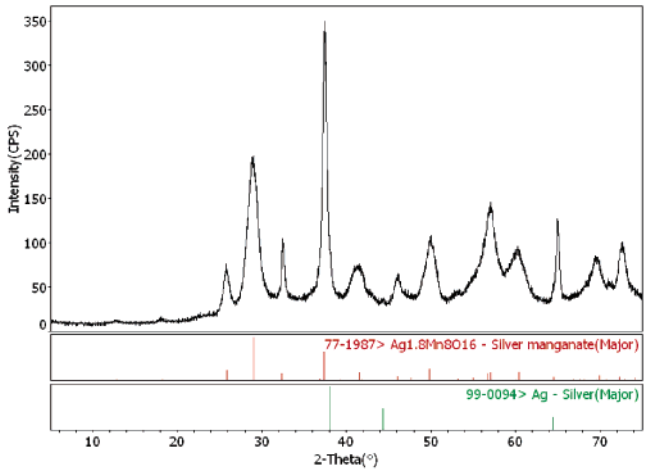


**Figure 6.** XRD pattern of Ag-hollandite from method B (Ag-hollandite B).

phase was removed from the final product, cryptomelane remains as the primary phase. This suggests that, despite the exchange procedure, there remains sufficient $K^+$ to dictate the final structure. It appears that the final calcination step does not change the structure of the product from cryptomelane to Ag-hollandite unless there is excess $AgNO_3$ present.

In synthesis method A described above, the calcination procedure was to heat in air from 25 to 500 °C at 10 °C/min and then maintain the temperature at 500 °C for 2 h. Under this procedure, the extra $AgNO_3$ first melts (at ~212 °C) and then decomposes (at ~444 °C) to Ag. It appears likely that the formation of the high-crystallinity Ag-hollandite structure occurs from 212 to 444 °C in the $AgNO_3$ melt. Consistent with this, an alternate method for Ag-hollandite synthesis, method B, i.e., cryptomelane ion-exchanged in $AgNO_3$ melt at 250 °C, was developed.

Figure 6 shows the XRD pattern of Ag-hollandite from method B (Ag-hollandite B). Figure 7 shows the TEM image along with the EDS spectrum, and Figure 8 shows the XPS spectrum of Ag in Ag-hollandite B. The chemical composition of Ag-hollandite B is given in Table 1. All these

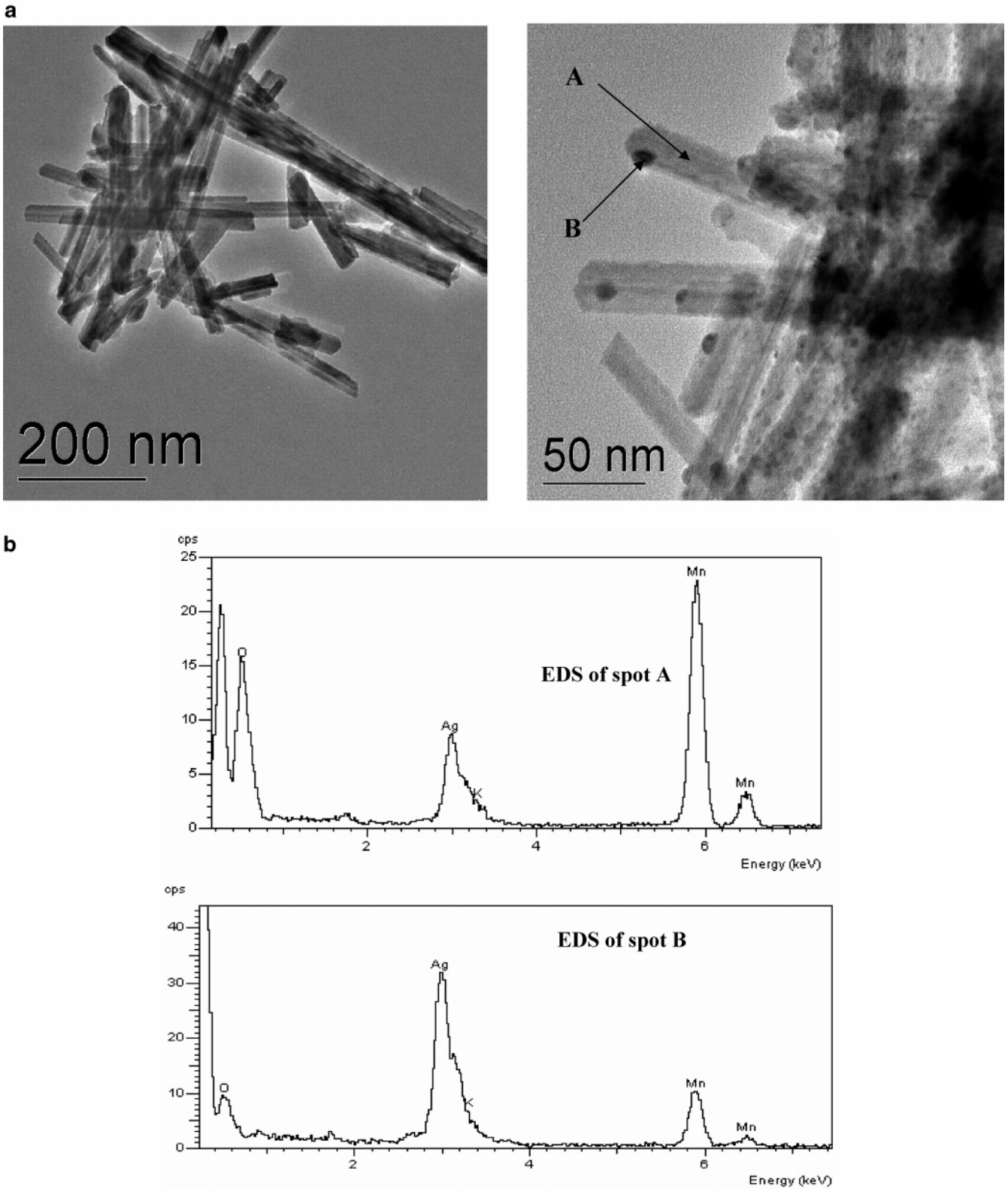


**Figure 7.** TEM image and selected area EDS spectrum of Ag-hollandite from method B. Small Ag particles are found on the Ag-hollandite surface (spot B EDS). Note that the EDS signal ratio of Ag/Mn in spot A (Ag-hollandite crystal without Ag metal phase) is larger than that in Figure 3, indicating the Ag concentration in this new Ag-hollandite is higher than that in the previous sample.

characterizations indicate that a much purer, well-crystallized Ag-hollandite can be synthesized via method B. Compared to the Ag-hollandite from method A, Ag-hollandite from method B has some different properties: (1) the XRD pattern shows only a barely noticeable amount of Ag; (2) the crystal size is slightly larger than that from method A and almost the same as that of starting cryptomelane material; (3) some very small silver particles (<5 nm diameter) were found coated on the Ag-hollandite surface, which was not seen on the Ag-hollandite A sample; (4) the $K^+$ concentration is significantly lower, which indicates the ion exchange between Ag and K cations is much more complete. A small amount

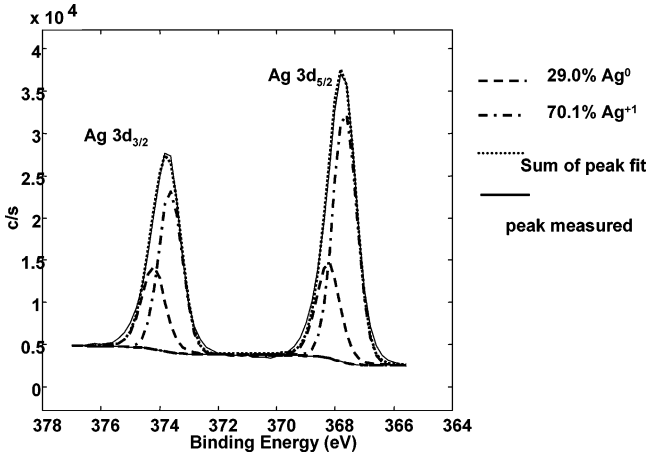


**Figure 8.** XPS of Ag-hollandite from synthesis method B (Ag-hollandite B). Two oxidation states of Ag ($Ag^0$ and $Ag^+$) coexist in this Ag-hollandite. Since XPS is a surface analysis technique (approximately several nanometers in depth), the ratio of these two states from XPS does not represent that of the bulk material.

of Ag particles were also found in a Ag-hollandite sample synthesized in $AgNO_3$ melt at 210 °C. It appears that Ag-hollandite free of trace Ag metal impurity cannot be obtained using the methods reported in this paper.

Like cryptomelane, the Ag-hollandite is quite stable under oxidation conditions. When heated in air, its structure remains unchanged up to 700 °C. However, under reducing conditions, it demonstrates high reactivity and lower thermal stability. Figure 9 provides the TPR traces of cryptomelane and Ag-hollandite B generated with 10% $H_2$ in Ar. Ag-hollandite from method A gives a TPR trace similar to that of Ag-hollandite B. $H_2$ reacts with Ag-hollandite as low as 100 °C, whereas cryptomelane reacts with $H_2$ above 250 °C. The products of reaction are MnO and elemental silver (in the case of silver hollandite). This unique property of Ag-hollandite is related to its facility in catalyzing certain low-temperature oxidation reactions.

**2. Low-Temperature $SO_2$ Absorption by Ag-Hollandite.** Previously, we reported that cryptomelane is an excellent $SO_x$ absorbent for diesel engine emission control.[21] At 325 °C and 8000 $h^{-1}$ GHSV, it absorbs more than 70 wt % $SO_2$ by oxidizing $SO_2$ to $SO_3$ and forming $MnSO_4$. However, at low temperature, its $SO_x$ capacity is greatly reduced. Since Ag-hollandite shows much higher reactivity in reductive gases at low temperature, it should be a better low-temperature $SO_2$ absorbent than cryptomelane. Figure 10 shows the $SO_2$ absorption curve for Ag-hollandite from method B and Table 2 compares its low-temperature $SO_2$ absorption performance with other absorbents tested. Compared to cryptomelane, Ag-hollandite shows much higher $SO_2$ capacity at low temperatures. Ag-hollandite from method B has $SO_2$ breakthrough capacity of 8.75 wt % at 150 °C and 26.8 wt % at 200 °C. Ag-hollandite from method A also shows much higher low-temperature $SO_2$ capacity (28 wt % at 250°) than that of cryptomelane, but less than that of Ag-hollandite B. Further work is required to explain the differences in performance between the two samples. The poor low-temperature performance of sample A that had $AgNO_3$ removed prior to calcination (see Table 2) is consistent with the low fraction of Ag-hollandite in the absorbent sample. Following $SO_2$ absorption by Ag-hollandite, XRD indicates that $MnSO_4$ is produced along with $Ag_2SO_4$. To our knowledge, Ag-hollandite is the best low-temperature $SO_2$ absorbent that has been identified. Combined with cryptomelane, a high-capacity $SO_x$ trap that is active at both low temperatures (~150 °C) and high temperatures (~550 °C) can be developed.

**3. Low-Temperature CO Oxidation by Ag-Hollandite.** Ag-hollandite shows significant activity for low-temperature CO oxidation. Figure 11 shows CO conversion to $CO_2$ as a function of temperature at a GHSV of 30000 $h^{-1}$. The feed gas composition is 230 ppm NO, 500 ppm CO, 378 ppm $C_3H_6$, 15% $O_2$, balance $N_2$. The data were obtained after 1 h of reaction at each temperature with the same sample. For comparison, data from cryptomelane are also provided in Figure 11. Under the test conditions, Ag-hollandite B oxidizes more than 80% CO to $CO_2$ at 100 °C, whereas cryptomelane oxidizes less than 2% CO under the same conditions. This result is consistent with earlier work by Xia et al.[2] using Ag-doped cryptomelane (partially crystallized Ag-hollandite). The effect of $SO_2$ absorption on Ag-hollan-

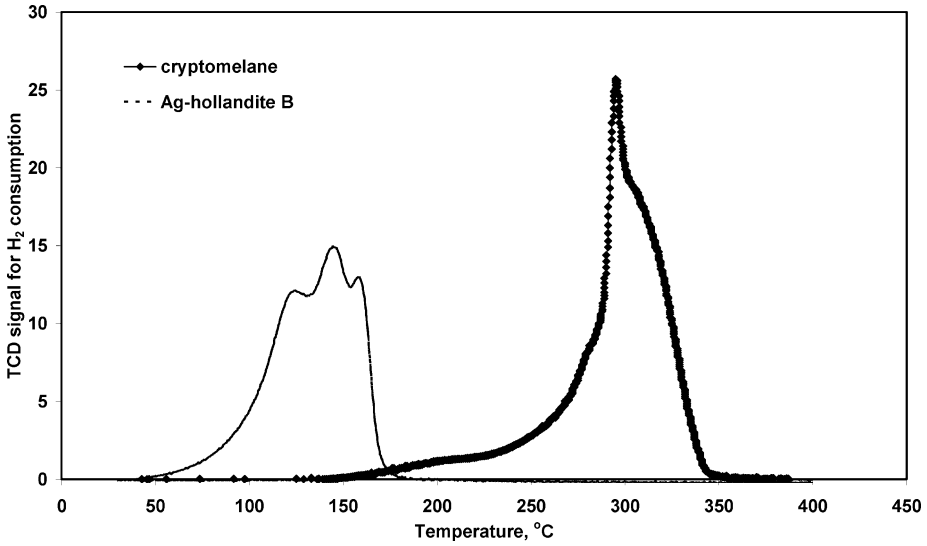


**Figure 9.** TPR results of cryptomelane (right) and Ag-hollandite B (left). TPR conditions: 40 sccm 10% $H_2$ in Ar, 10 °C/min from 25 to 600 °C.

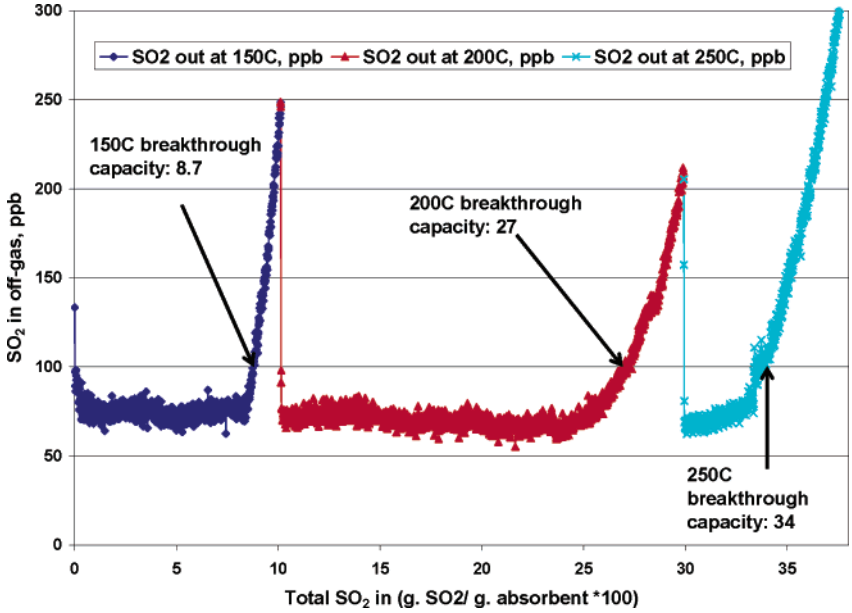


**Figure 10.** $SO_2$ absorption on Ag-hollandite B at different temperatures. Feed gas: 10 ppm $SO_2$ in air, 60000 $h^{-1}$ GHSV. After $SO_2$ breakthrough at low temperature, the same absorbent was tested at a higher temperature. Breakthrough capacity (100 × g. $SO_2$/g/absorbent) is defined as the point where $SO_2$ out exceeded 100 ppb.

**Table 2. $SO_2$ Breakthrough Capacity of Ag-Hollandites and Other Absorbents[a,b]**

| absorbent | 150 °C | 200 °C | 250 °C | 325 °C |
|---|---|---|---|---|
| cryptomelane | 1.54 | 1.60 | 2.90 | 63.85 |
| Ag-hollandite B | 8.75 | 26.84 | 33.52 | 42.5 |
| Ag-hollandite A | 2.20 | 5.20 | 38.1 | 43.3 (36[c]) |
| water-washed Ag-hollandite A | 1.71 | 1.71 | 4.12 | |

[a] Feed: 10 ppm $SO_2$ in air unless specified; GHSV: 60 K $h^{-1}$. [b] Breakthrough capacity (100 × g $SO_2$/g/absorbent): defined as the point where $SO_2$ out exceeded 100 ppb. [c] Feed gas: 10 ppm $SO_2$, 230 ppm NO, 500 ppm CO, 378 ppm $C_3H_6$, 15% $O_2$, balance $N_2$; GHSV: 60 K $h^{-1}$.

dite and cryptomelane oxidation capability is also different. With 8 ppm $SO_2$ in the feed, CO conversion over cryptomelane at 200 °C decreases from 100% to 60% over 15 h, whereas over the same period of time and with the same $SO_2$ concentration in the feed, conversion of CO over Ag-hollandite B at 150 °C remained unchanged at 100%. This difference is a result of the lower oxidation capacity of cryptomelane at low temperatures. Despite having more oxidation equivalents potentially available (as shown at higher temperatures), the rapid loss of the CO oxidation capacity of cryptomelane at 200 °C when $SO_2$ is simultaneously being absorbed suggests that both $SO_2$ oxidation and CO oxidation occur over the same sites. Consistent with this, fully $SO_2$-saturated Ag-hollandite does not have any CO oxidation activity. The low-temperature CO oxidation activity of Ag-hollandite compares favorably with noble metal-free, low-temperature CO oxidation catalysts.[2,22]

**4. NO Oxidation by Ag-Hollandite.** Ag-hollandite is also an active NO oxidation catalyst. Figure 12 shows its performance in oxidizing NO to $NO_2$ at different temperatures. The feed gas composition is 500 ppm NO, 300 ppm CO, 8.1% $O_2$, 1.7% $H_2O$, 7.2% $CO_2$, balance $N_2$. The GHSV is 30000 $h^{-1}$. The data were obtained after 30 min of reaction at each temperature. At 230 °C, silver hollandite oxidizes more than 85% NO to $NO_2$, which compares favorably with the performance of a conventional noble-metal-loaded NO oxidation catalyst (0.5 wt % $Pt/Al_2O_3$).[23] Above 288 °C, the conversion is limited by the thermodynamics of the reaction $NO + {}^1/_2\ O_2 \approx NO_2$. Ag-hollandite also exhibits some capability for de-$NO_x$ catalysis (conversion of $NO_x$ to $N_2$ in the presence of reductants). Under the conditions of the test, total $NO_x$ in the feed decreases by 15% at 250 °C (Figure 12 de-$NO_x$ curves). For comparison, NO conversion and de-$NO_x$ properties of cryptomelane were also measured and are provided in Figure 12. Cryptomelane is also a good catalyst for NO oxidation, although not as good as Ag-hollandite. However, cryptomelane does not show much de-NO activity, implicating the role of silver in the reaction.

The presence of Ag metal in both Ag-hollandite A and B makes it difficult to assign the oxidation activity toward CO and NO exclusively to the Ag-hollandite phase since metallic silver is a well-known oxidation catalyst.[24] The reported CO oxidation activity of nanocrystalline Ag supported on mesoporous silica,[25] under reaction conditions similar to those employed in our experiments, is insufficient to explain the activity observed with our materials, indicating that the silver hollandite phase must provide some if not all of the oxidation activity. On the other hand, the difference in performance between the A and B hollandite samples at low temperature could be due in part to the differences in Ag concentration and Ag particle size (i.e., metal surface area) for the two samples. It is most likely that both the Ag-hollandite and metallic Ag play a role in the low-temperature oxidation activity of the sample.

We observed no significant structural change in the silver hollandite samples after the CO and NO oxidation reactions

(21) Li, L. Y.; King, D. L. *Ind. Eng. Chem. Res.* **2005**, *44*, 168−177.
(22) Zheng, X. C.; Wang, S. P.; Wang, S. R.; Zhang, S. M.; Huang, W. P.; Wu, S. H. *Catal. Commun.* **2004**, *5*, 729−732.
(23) Muncrief, R. L.; Khanna, P.; Kabin, K. S.; Harold, M. P. *Catal. Today* **2004**, *98*, 393−402.
(24) Qu, Z. P.; Cheng, M. J.; Huang, W. X.; Bao, X. H. *J. Catal.* **2005**, *229*, 446−458.
(25) Liu, J.-H.; Wang, A.-Q.; Chi, Y.-S.; Lin, H.-P.; Mou, C.-Y. *J. Phys. Chem B Lett.* **2005**, *109*, 40−43.

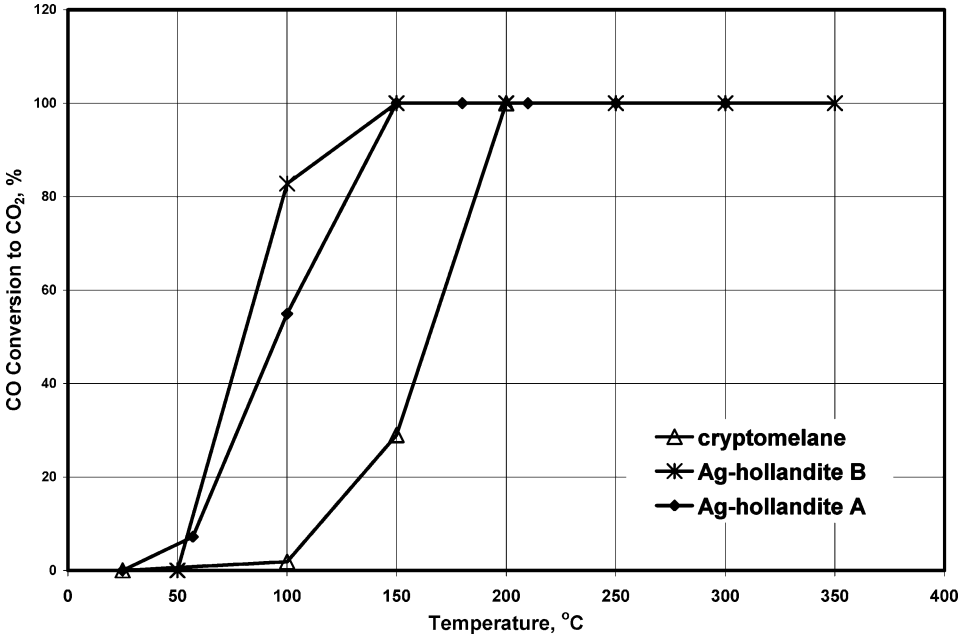


**Figure 11.** Catalytic oxidation of CO over Ag-hollandite A and B and cryptomelane. Feed gas composition: 230 ppm NO, 500 ppm CO, 378 ppm $C_3H_6$, 15% $O_2$, balance $N_2$. GHSV: 30000 $h^{-1}$. Data were collected after 1 h of reaction at each tested condition.

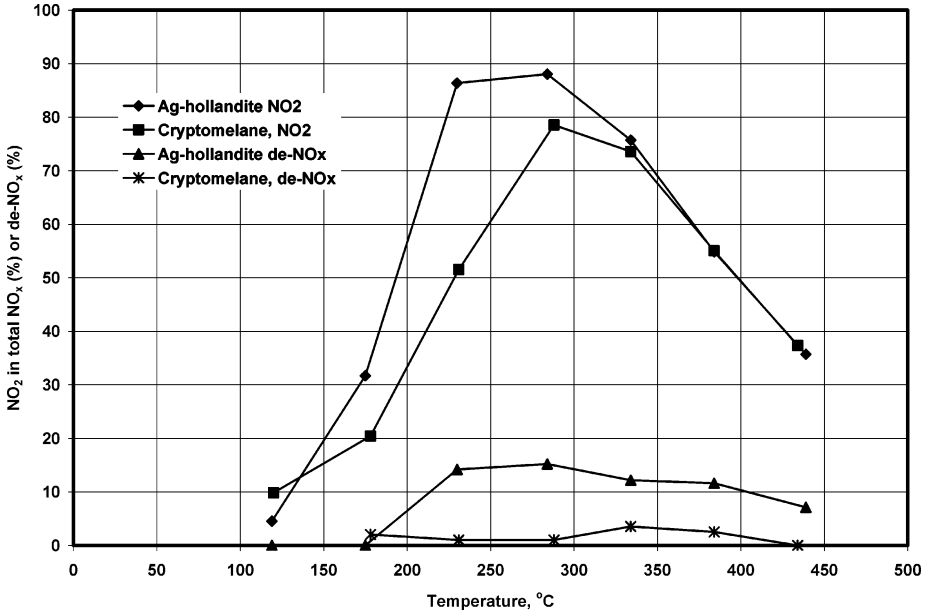


**Figure 12.** NO oxidation and de-$NO_x$ properties of Ag-hollandite A and cryptomelane. Feed gas: 500 ppm NO, 300 ppm CO, 8.1% $O_2$, 1.7% $H_2O$, 7.2% $CO_2$, balance $N_2$. GHSV: 30000 $h^{-1}$. Data were collected after 30 min at each tested condition.

so that this material must be a catalyst for these reactions rather than a stoichiometric oxidant. This is demonstrated in Table 2, which shows that Ag-hollandite A had 36 wt % $SO_2$ capacity at 325 °C when the exhaust gas contained CO, $C_3H_6$, and NO, compared with 43.3% $SO_2$ capacity in the absence of those reductants. If CO, NO, or $C_3H_6$ were able to reduce Ag-hollandite stoichiometrically, the $SO_2$ capacity would have been significantly decreased.

## Conclusions

High-crystallinity Ag-hollandite was successfully synthesized by post ion exchange of cryptomelane in an $AgNO_3$ melt. It appears that elevated temperatures in excess silver nitrate are required for extensive exchange of $K^+$ for $Ag^+$ and to achieve the structural conversion of cryptomelane to silver hollandite. Once formed, excess silver nitrate can be removed by washing. Compared to the previously described high-temperature solid-state syntheses process, this process is simple and the product has much smaller crystal size and much higher surface area. Ag-hollandite synthesized using this new process is an excellent low-temperature $SO_2$ absorbent, as well as a highly active catalyst for CO and NO oxidation. With CO−NO mixtures, silver hollandite also shows evidence of lean $NO_x$ catalytic activity, i.e., partial conversion of $NO_x$ to $N_2$.

**Acknowledgment.** Support of this work by the U.S. Department of Energy, Office of FreedomCAR and Vehicle Technolo-

gies, is gratefully acknowledged. This research was performed in part using the facility in the William R. Wiley Environmental Molecular Sciences Laboratory, a national scientific user facility sponsored by the U.S. Department of Energy's Office of Biological and Environmental Research and located at the Pacific Northwest National Laboratory. Pacific Northwest National Laboratory is operated by Battelle for the U.S. Department of Energy.

CM0506508